NeuroImage 62 (2012) 1354–1366

Contents lists available at SciVerse ScienceDirect

NeuroImage

journal homepage: www.elsevier.com/locate/ynimg

Investigating function and connectivity of morphometric findings — Exemplified on cerebellar atrophy in spinocerebellar ataxia 17 (SCA17)

Kathrin Reetz [a,b,c,*], Imis Dogan [a,b,c], Arndt Rolfs [e], Ferdinand Binkofski [a,b,c,d], Jörg B. Schulz [a,c], Angela R. Laird [f], Peter T. Fox [f], Simon B. Eickhoff [b,g]

[a] Department of Neurology, RWTH Aachen University, Pauwelsstrasse 30, D-52074 Aachen, Germany
[b] Institute of Neuroscience and Medicine, Research Center Jülich GmbH, Wilhelm-Johnen-Straße, D-52428 Jülich, Germany
[c] Jülich Aachen Research Alliance (JARA) — Translational Brain Medicine, Germany
[d] Division for Clinical and Cognitive Neuroscience, RWTH Aachen University, Pauwelsstrasse 30, D-52074 Aachen, Germany
[e] Medical Faculty, Albrecht-Kossel Institute for Neuroregeneration, University of Rostock, Rostock, Germany
[f] Research Imaging Center, University of Texas Health Science Center San Antonio, 7703 Floyd Curl Drive, San Antonio, TX 78229-3900, USA
[g] Institute of Clinical Neuroscience and Medical Psychology, Heinrich Heine University, Universitätsstr. 1, D-40225 Düsseldorf, Germany

ARTICLE INFO

Article history:
Accepted 22 May 2012
Available online 30 May 2012

Keywords:
Cerebellum
Meta-analytic connectivity modeling (MACM)
Spinocerebellar ataxia 17 (SCA17)
Voxel-based morphometry (VBM)

ABSTRACT

Spinocerebellar ataxia type 17 (SCA17) is a rare autosomal dominant neurodegenerative disorder characterized by progressive cerebellar ataxia but also a broad spectrum of other neuropsychiatric signs. As anatomical and structural studies have shown severe cerebellar atrophy in SCA17 and a differentiation of the human cerebellum into an anterior sensorimotor and posterior cognitive/emotional partition has been implicated, we aimed at investigating functional connectivity patterns of two cerebellar clusters of atrophy revealed by a morphometric analysis in SCA17 patients. In particular, voxel-based morphometry (VBM) revealed a large cluster of atrophy in SCA17 in the bilateral anterior cerebellum (lobule V) and another one in the left posterior cerebellum (lobules IX, VIIb, VIIIA, VIIIB). These two cerebellar clusters were used as seeds for functional connectivity analyses using task-based meta-analytic connectivity modeling (MACM) and task-free resting state connectivity analysis. Results demonstrated first consistent functional connectivity throughout the cerebellum itself; the anterior cerebellar seed showed stronger connectivity to lobules V, VI and to some extent I–IV, and the posterior cerebellar seed to the posterior lobules VI–IX. Importantly, the cerebellar anterior seed also showed consistently stronger functional connectivity than the posterior one with pre- and motor areas as well as the primary somatosensory cortex. In turn, task-based task-independent functional connectivity analyses revealed that the cerebellar posterior seed was linked with fronto-temporo-parietal areas as well as partly the insula and the thalamus, i.e., brain regions implicated in cognitive and affective processes. Functional characterization of experiments activating either cerebellar seed further corroborated this notion, revealing mainly motor-related functions for the anterior cluster and predominantly cognitive functions were associated for the posterior one.
The differential functional connectivity of the cerebellar anterior and posterior cluster highlights the manifold connections and dichotomy of the human cerebellum, providing additional valuable information about probably disrupted cerebellar–cerebral connections and reflecting the brunt of motor but also the broad spectrum of neuropsychiatric deficits in SCA17.

Introduction

The nature of cerebellar function and it's connections of different parts of the cerebellum are fundamental to understand it's functional organization. Traditionally, the cerebellum has been mainly considered dedicated to motor control. However, this view has been rather shifted and growing evidence for cognitive and affective function has emerged. Here, we exemplarily illustrate how to supplement specific functional information of current morphometric findings in the autosomal dominant spinocerebellar ataxia 17 (SCA17), a neurodegenerative disorder predominantly characterized by cerebellar atrophy and secondary degeneration of its connections. The diversity of impairments in SCA17 patients thus mirror the heterogeneity of functions ascribed to the cerebellum. Consequently, it stands to be reasoned, that distinct loci of atrophy in this disorder may potentially relate to the functional diversity within the cerebellum. While intuitive, this hypothesis however remains untested, as no study has yet attempted to link morphometric findings in this group to the physiological functions and connections of

* Corresponding author at: Department of Neurology, RWTH Aachen University, Pauwelsstrasse 30, D-52074 Aachen, Germany. Fax: +49 241 80 82139.
E-mail address: kreetz@ukaachen.de (K. Reetz).

1053-8119/$ – see front matter © 2012 Elsevier Inc. All rights reserved.
doi:10.1016/j.neuroimage.2012.05.058

the respective loci. SCA17 is caused by an expanded polyglutamine in the TATA-binding protein (TBP) (Koide et al., 1999; Nakamura et al., 2001) and aside from the clinical hallmark of cerebellar ataxia, the phenotypic spectrum of this disorder is highly variable and may comprise extrapyramidal motor symptoms (Hernandez et al., 2003; Nakamura et al., 2001; Zuhlke et al., 2001) such as dystonia (Hagenah et al., 2004; Hernandez et al., 2003), chorea (Toyoshima et al., 2004) and spasticity (Hagenah et al., 2004; Koide et al., 1999). SCA17 also manifests a broad spectrum of neuropsychiatric symptoms such as cognitive impairment, obsessive-compulsive personality disorder and phobia (Lasek et al., 2006; Maltecca et al., 2003; Rolfs et al., 2003). *Post mortem* examinations of SCA17 patients demonstrated cerebellar but also widely distributed cortical, and subcortical atrophy as well as cerebellar and cerebral cell loss and gliosis (Bruni et al., 2004). Previous magnetic resonance imaging (MRI) studies have demonstrated a marked and specific location of cerebellar atrophy in SCA17 patients, revealing structural alterations predominantly in the cerebellar posterior lobe, lobule VIII (Lasek et al., 2006) and lobule VIIA and the cerebellum anterior lobe (Reetz et al., 2010). At this, it has been demonstrated, that this cerebellar neurodegeneration is related to a variety of clinical motor features such as ataxia and extrapyramidal signs but also to a broad spectrum of neuropsychiatric symptoms (Lasek et al., 2006) and negatively correlated with the CAG trinucleotide repeat expansion size (Reetz et al., 2011). In particular, the motor-related neurodegeneration has been shown to be progressive in a longitudinal approach (Reetz et al., 2010).

These observations highlight the role of cerebellar atrophy in SCA17 but also raise questions about the secondary impact of these pathologies on other brain structures, given the dense, reciprocal connections between the cerebellum and telencephalic structures. In this context, it must be considered, that the traditional view holding motor control as the main function of the cerebellum has been extended to a variety of non-motor cerebellar functions (Bower, 1997; Burk et al., 2003; Schmahmann and Sherman, 1997; Timmann and Daum, 2007). Cerebellar contributions to cognitive and affective functions are moreover supported by a growing number of clinical, anatomical and functional neuroimaging studies (e.g. D'Agata et al., 2011a; O'Reilly et al., 2008; Ravizza et al., 2006; Schmahmann, 2004; Stoodley et al., 2012; Tedesco et al., 2011). Schmahmann and colleagues even formed the term of "cerebellar cognitive affective syndrome" including frontal, attentional, visuospatial, memory, language impairment and various affective and personality alterations (Schmahmann and Sherman, 1998). Consequently, it may be conjectured, that the phenotypical variety of SCA17 patients may arise from the disturbance of the cerebellar contribution to several distinct brain circuits. That is, the broad range of symptoms observed in SCA17 patients may primarily reflect a functional heterogeneity of the cerebellum and consequent affection of distinct functional networks by cerebellar atrophy. If this view holds, the loci of cerebellar atrophy observed in SCA17 patients should connect to both motor and cognitive domains of the cerebral cortex, potentially with a differentiation between the two distinct clusters revealed by morphometric analysis.

In this study, we aimed at testing this hypothesis by modeling the task-independent and task-based brain-wide functional connectivity (Eickhoff and Grefkes, 2011) of these two loci of cerebellar atrophy. In this context, task-independent functional connectivity-analysis is assessed using seed-based resting-state functional connectivity analysis, which allows to delineate brain regions showing coherent signal changes with the region of interest in an endogenously controlled "resting" state marked by the absence of explicit task demands. Functional connectivity in the context of externally purported tasks in turn is assessed by meta-analytic connectivity modeling (MACM), which assesses above-chance co-activation of a seed region across a large set of neuroimaging experiments (Laird et al., 2009a). Here, reference to the associated meta-data of tasks activating the seed also allows a behavioral characterization of the region of interest (cf. Eickhoff et al., 2011), rendering MACM a well-suited tool for the further assessment of morphological findings in terms of function and connectivity. This multi-modal approach should thus allow a comprehensive characterization of cerebello-cortical interactions of those regions atrophied in SCA17.

Methods

Brain morphometry assessment in SCA17 patients and healthy controls

The demographic and clinical characteristics of our sample of 16 SCA17 patients (mean age: 39.9 ± 12.6 SD years, 10 male; mean disease duration 10.8 ± 7.9; mean ICARS score 31.3 ± 25.5) and 16 age- and gender-matched healthy controls (mean age: 40.8 ± 10.8 SD years, 9 male) have been described in detail earlier (S-Table 1 in supplementary materials) (Lasek et al., 2006; Reetz et al., 2010, 2011). MR images for all subjects were re-analyzed using a voxel-wise statistical approach using SPM8 (www.fil.ion.ucl.ac.uk/spm). The following two approaches were performed:

A) For whole-brain analysis we used the voxel-based-morphometry toolbox (VBM8, http://dbm.neuro.uni-jena.de/vbm). Applying a probabilistic framework, images were registered using linear and non-linear transformations, segmented, and bias corrected within the same generative model (Ashburner and Friston, 2005). The following analyses were performed on gray matter segments that were multiplied by the Jakobian of the respective warp-fields (modulated gray matter volumes). Modulated gray matter images were smoothed with a Gaussian kernel of 8 mm full width at half maximum (FWHM). Additionally, we here used a cerebellar mask obtained from the WFU pickatlas (Maldjian et al., 2003).
B) For cerebellar VBM, we additionally used the Spatially Unbiased Infratentorial (SUIT) toolbox (version 2.5.3, http://www.icn.ucl.ac.uk/motorcontrol/ imaging/suit.htm), (Diedrichsen, 2006). To ensure that the infratentorial cerebellum was isolated from the surrounding tissue, we used the Isolate function within the SUIT toolbox, generating segmentation cerebellum maps. In the next step the cropped anatomical images were then normalized and the segmentation maps resliced into the SUIT atlas space. Finally, the homogeneity across the sample was checked and to preserve precision in the definition of cerebellar structures a smaller smoothing (i.e. 4 mm FWHM isotropic Gaussian kernel, which is in line with previous publications) was used (D'Agata et al., 2011b). All images were visually inspected to ensure that the pre-processing steps were successful and that the quality of each image was acceptable for subsequent analysis.

Using a general linear model, voxel-wise gray matter differences between SCA patients and controls were examined using a two-sample *t*-test. Similar to D'Agata et al., we tested two the two models on VBM and SUIT data (S-Table 2) (D'Agata et al., 2011b). To avoid possible edge-effects around the border between gray and white matter or cerebro-spinal fluid an absolute gray matter threshold of 0.01 (threshold masking) was used. For the statistical analysis, we employed a height threshold of $p<0.05$ family wise error (FWE) corrected with an extend threshold of k_E of 80 (=expected voxels per cluster) across the whole brain. We applied this rather conservative extend-threshold to ensure that a sufficient number of experiments could be obtained from the BrainMap database to facilitate the MACM analysis and functional characterization Given our focus on the cerebellum, only significant resulting cerebellar clusters were used as seed regions for functional connectivity analyses. Extra-cerebellar clusters can be found in the supplementary materials (S-Table 3).

Meta-analytic connectivity modeling (MACM)

Functional connectivity of the cerebellar seeds during structured task performance was delineated by meta-analytic connectivity modeling (MACM). This approach to functional connectivity assesses which brain regions are co-activated above chance with a particular seed region in functional neuroimaging experiments. It takes advantage of the fact that functional imaging studies are mostly reported in a highly standardized format using standard coordinate systems, and the emergence of large-scale databases, which store these information. The first step in MACM is to identify all these experiments in a database which activate the assessed seed region. After that quantitative meta-analysis is employed to test for convergence across the foci reported in these experiments indicating consistent co-activation (i.e., task-based functional connectivity) with the respective seed (Eickhoff et al., 2010; Robinson et al., 2010).

Using the BrainMap database (Laird et al., 2009a, 2011) (www.brainmap.org), we included only studies, which reported group analyses of functional mapping experiments of healthy subjects, yielding approximately 6,500 experiments for analysis. Experiments reporting between-group contrasts or effects of, e.g., pharmacological modulation, were not considered. To avoid a pre-selection bias and enable a completely data-driven approach, all eligible BrainMap experiments independent of behavioral categories were considered. To delineate task-based functional connectivity, i.e., co-activations of the clusters of cerebellar atrophy (Fig. 1A), we first identified all eligible (cf. above) experiments in the BrainMap database that reported at least one focus of activation in the respective seed (Fig. 1B). Subsequently, activation likelihood estimation (ALE) was used to identify consistent (across experiments) co-activations as reported in the retrieved experiments (Eickhoff et al., 2009b, 2010; Laird et al., 2009a, 2009b; Turkeltaub et al., 2002, 2012). This algorithm aims to identify areas showing a convergence of reported coordinates across experiments, which is higher than expected under a random spatial association. The key idea behind ALE is to treat the reported foci not as single points, but rather as centers for 3D Gaussian probability distributions capturing the spatial uncertainty associated with each focus based on an empirical model of between-subject and between-template variance (Eickhoff et al., 2009b). The probabilities of all foci reported in a given experiment were then combined for each voxel, resulting in a modeled activation (MA) map (Turkeltaub et al., 2012). Taking the union across these MA maps yielded voxel-wise ALE scores describing the convergence of results at each particular location of the brain. To distinguish 'true' convergence between studies from random convergence (i.e., noise), ALE scores were compared to an empirical null-distribution (Eickhoff et al., 2011) reflecting a random spatial association between experiments. Hereby, a random-effects inference is invoked, focusing on inference on the above-chance convergence between experiments, not clustering of foci within a particular study. The p-value of a "true" ALE was then given by the proportion of equal or higher values obtained under the null-distribution (Eickhoff et al., 2012). The resulting non-parametric p-values for each meta-analysis were then thresholded at a cluster-level FWE corrected threshold of $p<0.05$ (cluster-forming threshold at voxel-level $p<0.001$). Importantly, as experiments entering the ALE analysis were identified by featuring at least one focus of activation in the respective seed, any significant convergence outside the seed region should reflect consistent convergence of co-activations, i.e., task-based functional connectivity.

To contrast the functional connectivity of the different seed regions, we first calculated the voxel-wise differences of the Z-scores obtained from the inspected MACM-maps. The experiments contributing to either analysis were then pooled and randomly divided into two groups of the same size as the sets of contrasted experiments (Eickhoff and Grefkes, 2011; Eickhoff et al., 2012). Voxelwise ALE scores for these two randomly assembled groups were subtracted from each other and recorded. Repeating this process 10,000 times yielded an empirical null distribution of ALE-score differences between the two conditions. Based on this permutation-procedure, the map of true differences was then

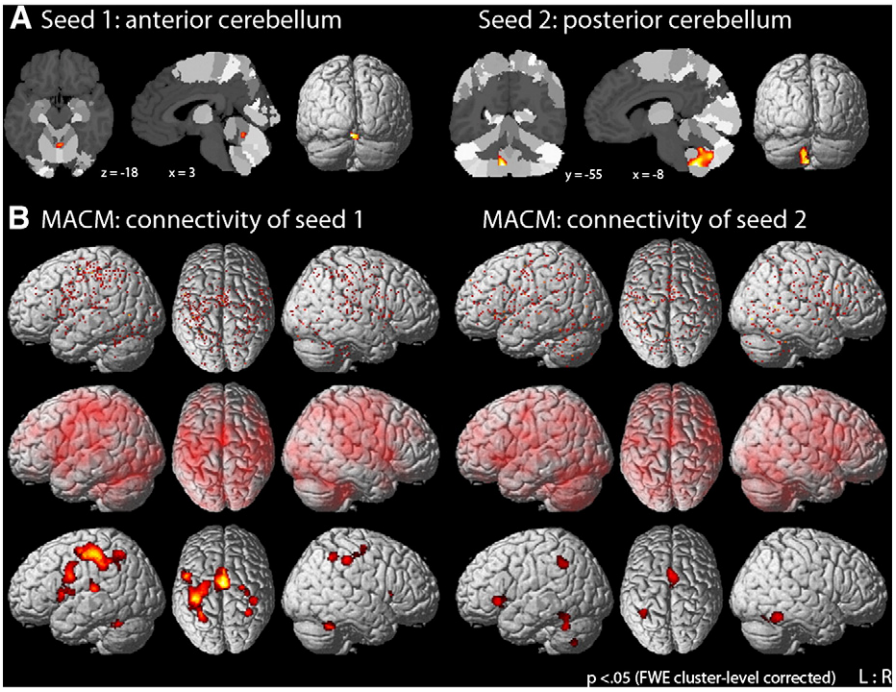

Fig. 1. Meta-analytic connectivity modeling (MACM). A) Location of the seed voxels in the anterior (cluster maxima in MNI space: 3/−58/−18) and posterior (−8/−55/−53) cerebellar clusters. B) Brain-wide co-activation maps of the seed voxels as revealed by MACM: Brain-wide foci reported in BrainMap that featured the closest activation peaks to the respective seed voxels (upper panel); these foci are modeled by 3D Gaussians reflecting uncertainty of their location using ALE meta-analysis (middle panel); above-chance convergence indicates significant co-activations with the respective cerebellar cluster (lower panel).

thresholded at a posterior probability of $p > .95$ for a true difference between the two samples (cluster extend threshold: $k_E \geq 20$ voxels, cf. Rottschy et al., 2012).

Task independent "resting state" connectivity modeling

Resting state fMRI images of 197 healthy volunteers (mean age 34.7 ± 20.0 [SD] years; 115 male) from the NKI/Rockland sample were obtained through the 1000 functional connectomes project (www.nitrc.org/projects/fcon_1000/). All subjects were visually inspected for complete cerebellar coverage, with the examined 197 subjects representing those of the total sample of 207 in which the cerebellum was sufficiently covered (complete coverage of the cerebellar hemispheres). During the resting state scans subjects were instructed to keep their eyes closed and to think about nothing in particular but not to fall asleep (which was confirmed by post-scan debriefing). For each subject 260 resting state EPI images were acquired on a Siemens TimTrio 3T scanner using blood-oxygen-level-dependent (BOLD) contrast [gradient-echo EPI pulse sequence, TR = 2.5 s, TE = 30 ms, flip angle = 80°, in plane resolution = 3.0 × 3.0 mm^2, 38 axial slices (3.0 mm thickness) covering the entire brain]. The first four scans were excluded from further processing analysis using SPM8. The EPI images were first corrected for movement artifacts by affine registration using a two pass procedure in which the images were first aligned to the initial volumes and subsequently to the mean after the first pass. The obtained mean EPI of each subject was then spatially normalized to the MNI single subject template using the 'unified segmentation' approach (Ashburner and Friston, 2005). The ensuing deformation was applied to the individual EPI volumes. To improve signal-to-noise ratio and compensate for residual anatomical variations images were smoothed by a 5-mm FWHM Gaussian.

The time-series data of each voxel were processed as follows (Jakobs et al., 2012): in order to reduce spurious correlations, variance that could be explained by the following nuisance variables was removed: i) the six motion parameters derived from the image realignment, ii) the first derivative of the realignment parameters, iii) mean gray matter, white matter and CSF signal per time-point as obtained by averaging across voxels attributed to the respective tissue class in the SPM8 segmentation, and iv) coherent signal changes across the whole brain as reflected by the first five components of a principal component analysis (PCA) decomposition of the whole-brain time-series (Behzadi et al., 2007). All nuisance variables entered the model as first and all but the PCA components also as second order terms as previously described by Behzadi et al. (2007) and shown by Chai et al. (2012) to increase specificity and sensitivity of the analyses. Data was then band pass filtered preserving frequencies between 0.01 and 0.08 Hz, since meaningful resting state correlations will predominantly be found in these frequencies given that the bold-response acts as a low-pass filter (Biswal et al., 1995; Fox and Raichle, 2007; Greicius et al., 2003). We again used the same seed regions as in the MACM analysis, i.e., the clusters of cerebellar atrophy identified from the morphometric study. Time-courses were extracted for all voxels within the particular cluster and expressed as their first eigenvariate. Linear (Pearson) correlation coefficients between the time series of the seed regions and all other gray matter voxel in the brain were computed to quantify resting-state functional connectivity (Zu Eulenburg et al., 2011). These voxel-wise correlation coefficients were then transformed into Fisher's Z-scores and tested for consistency in a flexible factorial model across subjects ($p < 0.05$ cluster-level FWE corrected, cluster-forming threshold at voxel-level $p < 0.001$).

Cross-validation of task-based MACM and task-free resting state functional connectivity

To detect areas showing task-dependent *and* task-independent functional connectivity with the seed regions, we performed a conjunction analysis between MACM and resting state analyses using the Nichols minimum statistics (Nichols et al., 2005). At this, we aimed at identifying voxels that showed significant functional connectivity with the seed in the analysis of interactions in both task-dependent and task-independent states. Practically, we delineated such consistent connectivity by computing the intersection of the connectivity maps from the two analyses.

Functional characterization

Functional characterization provides an important link between the morphometrically, i.e., structurally, defined seed-regions and putatively corresponding functional differentiation. Moreover, it may also provide hypotheses that may inform explicitly targeted further experiments. The functional characterization of our seeds was based on the BrainMap metadata that describes the included specific mental process isolated by the statistical contrast of each included experiment (Laird et al., 2011). Behavioral domains (BD) include the main categories of cognition, action, perception, emotion, interoception, as well as their related subcategories. The respective paradigm classes (PC) classify the specific task employed (a complete list of behavioral domains and paradigm classes can be found at http://brainmap.org/scribe/). We analyzed the behavioral domain and paradigm class metadata associated with each cluster of the morphometric findings to determine the frequency of domain "hits" relative to its likelihood across the entire database (Nickl-Jockschat et al., 2010, 2011). In particular, functional roles of the seeds were identified by significant over-representation of behavioral domains and paradigm class in the experiments activating the respective cluster relative to the BrainMap database using a binomial test ($p < 0.05$), corrected for multiple comparisons using Bonferroni's method (Laird et al., 2009a).

Anatomical allocation

All results were anatomically labeled by reference to probabilistic cytoarchitectonic maps of the human brain using the SPM Anatomy Toolbox (Eickhoff et al., 2005, 2007). Using a Maximum Probability Map (MPM), activations were assigned to the most probable histological area at their respective locations. Details on these cytoarchitectonic regions can be found in the following publications reporting on the cerebellum (Diedrichsen et al., 2009), thalamic connectivity zones (Behrens et al., 2003), hippocampus (Amunts et al., 2005), premotor cortex (PMC, BA 6; Geyer, 2004), primary motor cortex (M1, BA 4a, 4p; Geyer et al., 1996), primary somatosensory cortex (SI, BA 3, 1, 2; Geyer et al., 1999, 2000), secondary somatosensory cortex (SII: OP1, OP4; Eickhoff et al., 2006), Broca's region (Amunts et al., 1999), inferior and superior parietal cortex (IPC and SPC; Caspers et al., 2008; Scheperjans et al., 2008), intraparietal sulcus (IPS; Choi et al., 2006; Scheperjans et al., 2008), posterior insula (Kurth et al., 2010a), and visual cortex (Amunts et al., 2000; Rottschy et al., 2007) .

Results

Voxel-based morphometry

The morphometric analysis revealed two distinct clusters of cerebellar atrophy in SCA17 patients compared to controls that were used as seed voxels for further analysis (Fig. 1A). The first cluster involving 927 voxels was predominantly located in the left-sided cerebellar posterior lobe, lobule IX (left = 51% of the cluster volume attributed to this structure, main maximum at the coordinates x = −8, y = −55, z = −53) extending to the lobules VIIIA and VIIIB (21% attributed to this structure) as well as the lobule VIIb (3%). The second cluster containing 104 voxels was localized in the bilateral cerebellar anterior lobe, lobule V (right = 54%, left = 45%, main max. x = 3, y = −58, z = −18).

Meta-analytic connectivity modeling

Meta-analytic connectivity modeling using the anterior cerebellar cluster as seed-region revealed above-chance convergence, indicating significant co-activations, bilaterally in lobules VI and V of the bilateral cerebellum encroaching the fusiform gyrus (Table 1, Fig. 1B). Cortically, significant co-activations were found not only in bilateral motor (M1: BA 4a, 4p), premotor (PMC: BA6) cortices and the bilateral supplementary motor area (SMA: BA 6), but also in the primary somatosensory (SI: BA 3a, 3b, 1, 2) and adjacent parietal cortices (IPS: hIP1-3; IPC: PFt, PFop, PFcm; SPC: 7A, 7PC). Additionally we found significant connectivity in the midcingulate cortex, left Broca's areas (BA 44) extending to the anterior-dorsal insula as well as the parietal operculum (OP1). Co-activations in subcortical nuclei included the right pallidum, the bilateral putamen and the thalamus, predominantly in regions connecting to the prefrontal cortex, but also parietal, temporal and motor cortices (Behrens et al., 2003).

The MACM map for the cerebellar posterior seed cluster revealed significant co-activations bilaterally within the posterior cerebellum (mainly in lobules VI–IX), in the left inferior frontal gyrus, anterior-ventral insula, midcingulate cortex and bilateral SMA (BA 6). We further found co-activations in the bilateral fusiform gyrus, the inferior temporal gyrus, the left IPS (hIP1-3) and mainly in prefrontal connectivity zones of the bilateral thalamus (Behrens et al., 2003), (Table 1, Fig. 1B).

A conjunction analysis (cf. Caspers et al., 2010) revealed an overlap between the thresholded ($p<0.05$, cluster-level FWE corrected) co-activation maps of both clusters and hence functional connectivity with both seed regions in the bilateral cerebellar lobule VI, SMA (BA 6), left midcingulate cortex, fusiform gyrus, the IPS (hIP1, hIP3), as

Table 1
Task-dependent MACM functional connectivity.

Cluster #	k_E	MNI co-ordinates[a]			Lat.	Macroanatomical and cytoarchitectonic region
		x	y	z		
Anterior cerebellar seed						
Cluster 1	2544	2	−60	−18	R	Cerebellum [lobules: 26% VI; 16% V; 2% VIIIA; 1.5% I–IV];
					L	Cerebellum [lobules: 26% VI; 13% V; 3% I–IV; 1% VIIIB];
					L/R	Fusiform gyrus
Cluster 2	1700	−38	−32	48	L	Postcentral gyrus, SI [BA 3a, 3b, 1, 2]; superior frontal gyrus; precentral gyrus, PMC [BA 6], M1 [BA 4a, 4p]; intraparietal sulcus [hIP1, hIP2, hIP3]; angular gyrus; superior parietal lobule [7A, 7PC]; inferior parietal cortex [PFt]
Cluster 3	1374	2	−8	58	L/R	Precentral gyrus, SMA [BA 6]; middle cingulate cortex
Cluster 4	524	−14	−24	11	L/R	Thalamus
Cluster 5	371	−54	2	26	L	Inferior frontal gyrus [BA 44]; precentral gyrus, PMC [BA 6], M1 [BA 4a, 4p]; postcentral gyrus, SI [BA 3a, 3b]
Cluster 6	335	−38	8	12	L	Inferior frontal gyrus [BA 44]; insula; putamen
Cluster 7	271	40	−32	46	R	Postcentral gyrus, SI [BA 3a, 3b, 2]; precentral gyrus, PMC [BA 6], M1 [BA 4a, 4p]; inferior parietal cortex [PFt]; intraparietal sulcus [hIP2]
Cluster 8	197	30	12	8	R	Pallidum; putamen; insula
Cluster 9	149	−52	−26	14	L	Parietal operculum, SII [OP 1]; Heschl's gyrus [TE 1.1, 1.0]; inferior parietal cortex [PFop, PFcm]; superior temporal gyrus
Cluster 10	122	36	−48	48	R	Intraparietal sulcus [hIP3, hIP2]; superior parietal lobule [7PC]; postcentral gyrus, SI [BA 2]
Posterior cerebellar seed						
Cluster 1	1109	−10	−70	−38	L	Cerebellum [lobules: 20% VIIIA, 10% VIIIB; 10% VIIb; 11% IX; 6% VIIa (Crus I, II); 3% VI]
					R	Cerebellum [lobules: 1.5% VIIIA, VIIIB, IX]
Cluster 2	450	4	0	56	R	Precentral gyrus, SMA [BA 6]
					L	Precentral gyrus, SMA [BA 6]; middle cingulate cortex
Cluster 3	267	−12	−20	6	L	Thalamus
Cluster 4	213	−40	−52	−30	L	Cerebellum [22% VI; 23% VIIa, Crus I]; fusiform gyrus; inferior temporal gyrus
Cluster 5	204	44	−50	−18	R	Fusiform gyrus; inferior temporal gyrus; cerebellum [3% VI]
Cluster 6	203	−42	26	0	L	Inferior frontal gyrus, p. triangularis and orbitalis; anterior insula
Cluster 7	183	−36	−54	40	L	Intraparietal sulcus [hIP1, hIP2, hIP3]
Cluster 8	154	14	−60	−22	R	Cerebellum [lobule: 89% VI]
Cluster 9	127	12	−18	6	R	Thalamus
Conjunction: anterior and posterior cerebellar seed						
Cluster 1	352	2	0	56	R	Precentral gyrus, SMA [BA 6];
					L	Precentral gyrus, SMA [BA 6]; middle cingulate cortex
Cluster 2	214	−12	−20	6	L	Thalamus
Cluster 3	48	14	−60	−22	R	Cerebellum [lobule: 99.5% VI]
Cluster 4	47	−36	−46	46	L	Intraparietal sulcus [hIP1, hIP3]
Cluster 5	20	−36	−54	−26	L	Cerebellum [lobule: 68% VI]; fusiform gyrus
Contrast: anterior > posterior cerebellar seed						
Cluster 1	928	6	−60	−26	R	Cerebellum [lobules: 35% V; 22% VI; 2% I–IV]
					L	Cerebellum [lobules: 18% V; 11% VI; 2% I–IV]
Cluster 2	508	−38	−24	48	L	Postcentral gyrus, SI [BA 3a, 3b, 1, 2]; precentral gyrus, M1 [BA 4a, 4p], PMC [BA 6]; inferior parietal cortex [PFt]
Cluster 3	46	40	−32	42	R	Postcentral gyrus, SI [BA 2]; intraparietal sulcus [hIP2]
Cluster 4	40	−6	−16	46	L	Precentral gyrus, SMA [BA 6]
Cluster 5	25	28	−14	50	R	Precentral gyrus, PMC [BA 6]
Contrast: anterior < posterior cerebellar seed						
Cluster 1	968	−10	−72	−44	L	Cerebellum [lobules: 18% VIIIA, 12% IX; 11% VIIb; 9% VIIIB; 7% VIIa (Crus I, II); 3% VI]
Cluster 2	155	−36	24	−2	L	Inferior frontal gyrus; anterior insula
Cluster 3	133	44	−52	−20	R	Fusiform gyrus; Inferior temporal gyrus
Cluster 4	31	14	−14	6	R	Thalamus

k_E: cluster extent; Lat.: laterality; L: left; R: right; M1: primary motor cortex; PMC: premotor cortex; SMA: supplementary motor area; SI: primary somatosensory cortex; SII: secondary somatosensory cortex.

[a] Cluster maxima.

well as in the a part of the left thalamus connecting to the prefrontal cortex (Table 1, Fig. 2A).

Contrasting the co-activation maps for the two clusters, the anterior cluster showed significantly higher co-activation probabilities mainly in cerebellar lobule V and to a lesser extent in lobule VI, in the bilateral primary somatosensory cortex (BA 2, left BA 3a, 3b, 1), PMC (BA 6), left M1 (BA 4a, 4p) and SMA (BA 6), as well as in anterior parietal regions (left IPC: PFt; right IPS: hIP2). In contrast, the posterior cluster showed significantly higher co-activation probabilities in left posterior cerebellar lobules (particularly VIIa (Crus I, II), VIIb, VIIIA, VIIIB and IX), left inferior frontal and anterior-ventral insular cortex, right occipito-temporal cortex and thalamic regions connecting to the prefrontal cortex (Table 1, Fig. 2B).

Functional characterization of seed-regions

Behavioral domains, paradigm classes and experimental conditions that were significantly overrepresented in experiments activating the cerebellar anterior cluster relative to the BrainMap database were mostly related to motor functions (i.e., action, action execution, finger tapping, instruction of movement), except for the overrepresentation of the recall in sequence learning tasks, which, however, often also requires motor activity (e.g., key presses). The posterior cluster showed less functional specificity, but was predominantly associated with attention-related cognitive tasks (i.e., action observation, instruction of attention). No specific paradigm classes were significantly overrepresented among experiments activating the posterior seed (Fig. 2C).

Resting-state connectivity modeling

To consolidate the differential connectivity patterns of the cerebellar anterior and posterior cluster, as indicated by MACM, we further performed a resting-state functional connectivity analysis in an independent dataset of 197 healthy subjects (Table 2, Fig. 3).

Resting state connectivity with the cerebellar anterior cluster revealed one large cluster in the bilateral cerebellum (predominantly lobules VIIa (Crus I, II), VI and to a lesser extent V) extending bilaterally to the caudate, putamen, pallidum, thalamus (mainly prefrontal, but also premotor and right somatosensory connectivity zones) and visual cortex (V3v, V4, BA 18). We further found significant resting state connectivity with the anterior seed in bilateral motor and somatosensory cortices (M1: BA 4p, 4a; PMC and SMA: BA 6; SI: BA 3b, 3a, 1, 2), in superior and middle frontal gyri, the left anterior cingulate cortex and right posterior insula (Ig2) extending to the parietal operculum (OP1, OP4). Two significant clusters were located in the bilateral hippocampus (CA, FD) and adjacent parahippocampal gyrus (Table 2, Fig. 3A).

The cerebellar posterior seed showed significant connectivity with mainly lobules VIIa (Crus I, II) and VI within the cerebellum. Cortically, one large right-sided cluster was found in the superior and middle frontal gyrus, extending to mid-orbital and superior medial parts as well as the SMA. Further cortical clusters were located in the right IPC (PGp, PGa), SPC (7A, 7P, 7M), precuneus, middle temporal gyrus and left superior frontal gyrus (Table 2, Fig. 3B).

As revealed by conjunction analysis, regions commonly correlated, i.e., functionally connected, with both cerebellar seeds were found mainly in cerebellar lobules VIIa (Crus I, II) and VI (Table 2, Fig. 3C). Contrasting the resting state connectivity of both seeds confirmed the above-described pattern of single resting state connectivity analyses. The anterior seed more strongly correlated with lobules V, VI and I–IV in the cerebellum, the thalamus, striatum, hippocampus (CA, FD) and adjacent parahippocampal gyrus. Cortically, stronger resting state connectivity of the anterior seed was shown in bilateral motor and somatosensory cortices (M1, PMC, SMA, SI), left middle and superior frontal gyrus, anterior cingulate, right posterior insula and parietal operculum (OP1, OP4), and visual cortices. In contrast, the posterior seed more strongly correlated with posterior cerebellar lobules (mainly VIIa (Crus I, II) and IX), with orbital and medial regions of the frontal lobe, inferior and superior parietal areas, the precuneus, and middle temporal gyrus (Table 2, Fig. 3D).

Cross-validation of task-based MACM and task-free resting state functional connectivity

In the conjunction analysis of both task-based (MACM) and task-independent (resting-state) approaches, we found significant functional connectivity of the cerebellar anterior seed with the bilateral cerebellar lobules VI and V, motor and somatosensory cortices (M1, PMC, SMA, SI) and the thalamus (prefrontal connectivity zone). The cerebellar posterior seed showed significant connectivity, across both approaches, with bilateral posterior lobules within the cerebellum (lobules VI–IX). Hence, this finding indicates that particularly sensorimotor and thalamic areas show functional connectivity with the cerebellar anterior seed across two fundamentally different states (i.e., during task performance and during resting state), while consistent functional connectivity of the posterior seed seems to be restricted to cerebellar posterior areas. Again, this finding was confirmed when we calculated the conjunction between MACM and resting state connectivity for the difference maps of both seeds, respectively (Table 3).

Discussion

Task-based MACM and task free resting state functional connectivity analyses of two cerebellar clusters showing significant atrophy in SCA17 patients relative to healthy controls, demonstrate differential connectivity patterns and functional characterization. We found high functional connectivity throughout the cerebellum itself; the cerebellar anterior seed showed stronger connectivity to lobules V, VI and to some extent I–IV, and the posterior cerebellar seed to the posterior located lobules VIIIA, VIIIB, VIIa, VIIb and IX. Importantly, we revealed that the cerebellar anterior seed was associated with stronger consistent functional connectivity in motor-related areas but also the primary somatosensory cortex. Whereas the conjunction of task-based and task-independent resting state connectivity modeling failed to demonstrate consistent cortical functional connectivity, they both revealed an interaction of the cerebellar posterior seed with more cognitive-related fronto-temporo-parietal areas as well as the insula, respectively.

Connectivity and function of the anterior cerebellar region atrophic in SCA17

Our first cluster was found in the anterior lobe, in lobule V. Consistent connectivity in both task-dependent and task-independent states for this anterior cerebellar seed was observed within the cerebellum and the cortex. In the cerebellum, functional connectivity was noticed in cerebellar lobules I–VIII with a focus on lobules V and VI. Cortically, consistent functional connectivity was found with the bilateral precentral gyrus including M1, the PMC and extending to SI on the postcentral gyrus, as well as with the thalamus.

Based on previous studies, a dichotomy of the human cerebellum into an anterior sensorimotor and posterior cognitive/emotional part has been proposed (Stoodley and Schmahmann, 2009) and that there seem to be separate cerebro-cerebellar circuits for cognitive as well as motor operations (Kelly and Strick, 2003). At this, it has to be noted that cortico-cerebellar connections, as shown by Kelly and Strick, demonstrate that M1 projects to lobules V, VI, VIIb, and VIII, while area 46 projects to VIIa (Kelly and Strick, 2003). This implies that M1 and area 46 are interconnected with separate regions of the cerebellar cortex. The observed functional connectivity pattern resonates very well with the hypothesis, that in particular the anterior cerebellar lobes, i.e., the location of the currently discussed cluster, have been shown to be fundamentally involved in motor control (Exner et al., 2004; Levisohn et al., 2000; Schmahmann, 2004; Schmahmann and

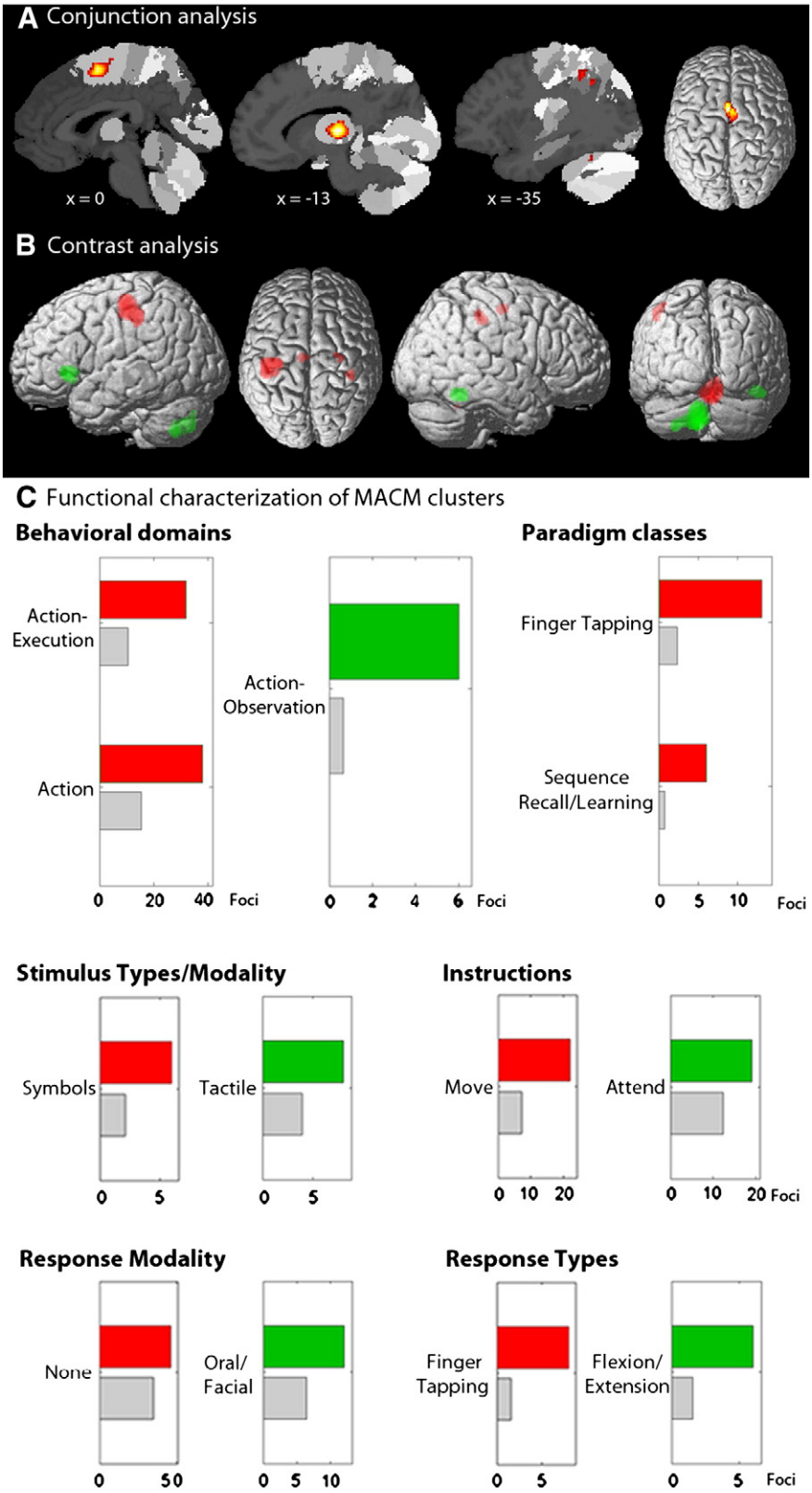

Fig. 2. Meta-analytic connectivity modeling (MACM) and functional characterization. A) Conjunction analysis over the MACM maps for the two cerebellar clusters indicates that the SMA, midcingulate, thalamus, cerebellar lobule VI and parietal regions significantly co-activate with both the anterior and posterior cerebellar cluster. B) Contrasting the MACM maps for the two clusters, the anterior cluster showed higher co-activation probabilities mainly in the cerebellar lobule V and in sensorimotor and parietal cortices (red blobs). The posterior cluster showed significantly higher co-activation probabilities with the posterior cerebellum, thalamus, as well as inferior frontal, anterior insular and occipito-temporal cortices (green blobs). C) Functional Characterization by behavioral domain, paradigm class and experimental conditions metadata. The red/green bars denote the number of foci for that particular label within the anterior/posterior cluster. The gray bars represent the by-chance frequency of one label given the size of the cluster, and denote the number of foci that would be expected to hit the particular cluster if all foci with the respective domain were randomly distributed throughout the cortex. Overall, the anterior cluster was strongly related to motor functions, while the posterior cluster showed less specificity but was predominantly associated with attention-related cognitive tasks.

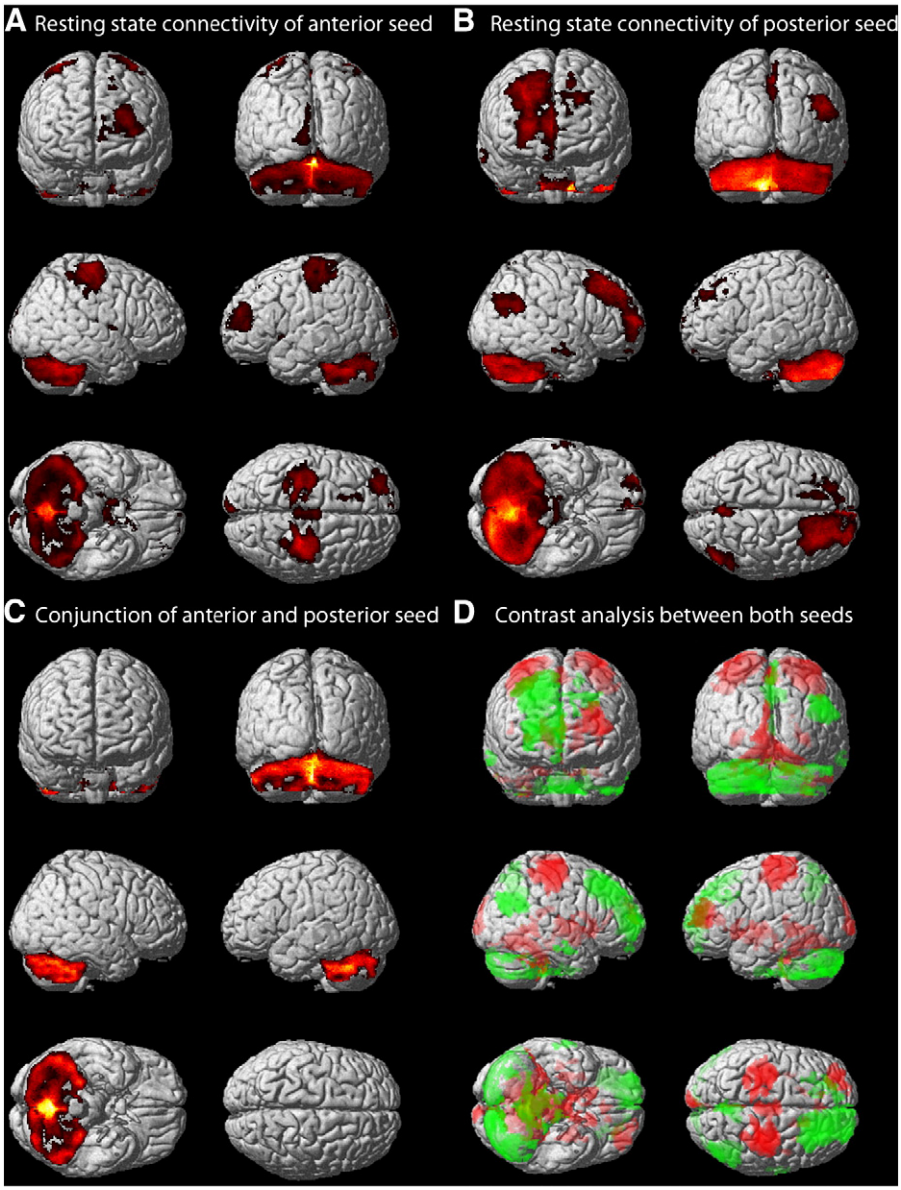

Fig. 3. Resting state connectivity. A) Resting state connectivity with the anterior cerebellar cluster was observed mainly in lobules V–VII within the cerebellum extending to the striatum, pallidum, thalamus and hippocampus. Cortically, significant correlations were mainly found in motor and sensorimotor regions (M1, PMC, SMA, SI), and further superior and middle frontal gyri, anterior cingulate cortex and posterior insula. B) For the posterior cluster significant resting state correlation was found mainly with posterior cerebellar lobules, with frontal gyri extending to mid-orbital and superior medial parts as well as the SMA in the frontal lobe. Further cortical clusters were located in parietal areas, the precuneus and middle temporal gyrus. C) Conjunction analysis between both cerebellar seeds showed common connectivity only within the cerebellum, mainly in posterior lobules. D) Contrasting the connectivity maps for the two clusters, the anterior cluster showed higher connectivity particularly with anterior cerebellar lobules, the thalamus, hippocampus, striatum, and motor as well as sensorimotor areas, frontal gyri, anterior cingulate, posterior insula and parietal operculum (red blobs). The posterior cluster was more strongly correlated with posterior cerebellar lobules, orbital and medial regions of the frontal lobe, inferior and superior parietal areas, the precuneus, and middle temporal gyrus (green blobs).

Sherman, 1998; Schoch et al., 2006; Tavano et al., 2007). In particular, for lobules III–VI evidence for the sensorimotor homunculi was provided by physiological recordings in animals (Snider and Eldred, 1951) and functional neuroimaging studies in humans (Grodd et al., 2001). A previous meta-analysis of fMRI studies revealed that motor-related tasks in neuroimaging studies were localized in the anterior lobe, with a secondary representation in lobules VIIIA/B and somatosensory-related tasks also involved the anterior lobe, with a secondary representation in lobule VIIIB (Stoodley and Schmahmann, 2009). In more detail, motor and somatosensory representations exhibited a largely overlapping pattern, mainly focused in lobule V and the adjacent part of lobule VI. The strong connectivity between lobules V and VI and motor cortical regions confirms previous findings, which have been repeatedly shown in resting state studies (Buckner et al., 2011; Habas et al., 2009; O'Reilly et al., 2010). Our data demonstrate, that the cerebellar anterior cluster was highly connected within most of the functionally motor-related cerebellar anterior lobe. Their disturbance may cause the cerebellar dysfunction leading to the clinical motor impairment in SCA17, in particular to the pathognomical feature of cerebellar ataxia. Consistent functional connectivity of the cerebellar anterior seed, however, was not only found within the cerebellum, but also with the bilateral precentral gyrus including M1 and PMC and extending to the postcentral gyrus. These connections thus reflect predominantly motor-related cerebello-cerebral pathways, linking the cerebellum with key areas of cortical motor control (cf. Grefkes et al., 2008). In addition to consistent functional connectivity within the cerebellum and cerebello-cerebral connections, we moreover also found evidence for thalamic involvement in this potentially disrupted circuitry, revealing a network of cerebello-thalamo-cerebral connections for the

cerebellar anterior location of SCA17 atrophy. Matching this view, regions of the thalamus coupled with our anterior cluster were previously demonstrated to connect to the motor, prefrontal cortex and parieto-temporal cortices (Behrens et al., 2003). This emphasizes the thalamic function as the gateway to the telencephalon, routing motor and sensori-motor information arising from the cerebellum.

Although a convergent significant functional connectivity with the basal ganglia could not be sustained in the conjunction analysis of the task-based MACM and task free resting state functional connectivity analyses, both single analyses demonstrated functional connectivity mainly to the putamen, respectively. With the cerebellum, the basal ganglia constitute the two largest subcortical stations of motor system, with both operating often in parallel (cf. Eickhoff et al., 2009a). Although it is believed that the basal ganglia and cerebellum are both anatomically and functionally distinct (Graybiel, 2005), their direct interaction via the striatum (Hoshi et al., 2005) and/or the sub-thalamic nucleus (Bostan et al., 2010) is assumed. The dysfunction of the basal ganglia in the neurodegenerative disorder SCA17 has been

Table 2
Task-independent resting-state functional connectivity.

Cluster #	k_E	MNI co-ordinates[a]			Lat.	Macroanatomical and cytoarchitectonic region
		x	y	z		
Anterior cerebellar seed						
Cluster 1	41,564	0	−60	−16	L	Cerebellum [11% VIIa (Crus I, II); 11% VI; 4% V; 2% I–IV; 2% VIIIA, 1% VIIIB; 1% IX–X; 0.5% VIIb]; brainstem; thalamus; caudate; putamen; pallidum; visual cortex [hOC4v, V4; hOC3v, V3v; BA 18]
					R	Cerebellum [16% VIIa (Crus I, II); 11% VI; 4% V; 2% I–IV; 2% IX–X; 1% VIIb; 1% VIIIA, 1%VIIIB]; brainstem; thalamus; caudate; putamen; pallidum; hippocampus [SUB; HATA; CA]; visual cortex [hOC3v; BA 18]
Cluster 2	5043	32	−28	52	R	Precentral gyrus, M1 [BA 4p, 4a], PMC [BA 6]; postcentral gyrus, SI [BA 3b, 3a, 1, 2]; inferior parietal cortex [PFt]
Cluster 3	4098	−30	−32	58	L	Precentral gyrus, M1 [BA 4p, 4a], PMC [BA 6]; postcentral gyrus, SI [BA 3b, 3a, 1, 2]; superior parietal lobule [5L]
Cluster 4	2204	−22	50	24	L	Middle frontal gyrus; superior frontal gyrus
Cluster 5	1069	3	−28	56	R/L	Precentral gyrus, M1 [BA 4a], SMA [BA 6]
Cluster 6	752	−28	−39	−3	L	Hippocampus [CA; FD]; parahippocampal gyrus; Thalamus
Cluster 7	606	33	−52	−2	R	Hippocampus [CA]; parahippocampal gyrus
Cluster 8	509	−8	−104	0	L	Visual cortex [BA 17, 18]
Cluster 9	234	12	34	10	L	Anterior cingulate
Cluster 10	185	40	−12	6	R	Insula [Ig2]; parietal operculum, SII [OP1, OP4]
Cluster 11	181	−16	28	48	L	Superior frontal gyrus
Posterior cerebellar seed						
Cluster 1	41,741	−8	−60	−46	L	Cerebellum [22% VIIa (Crus I, II); 10% VI; 3% IX–X; 2% VIIIA, 1% VIIIB; 1% VIIb; 2% V; 1% I–IV]; brainstem
					R	Cerebellum [19% VIIa (Crus I, II); 9% VI; 3% IX–X; 2% VIIIA, 1% VIIIB; 1% VIIb; 2% V; 0.5% I–IV]; brainstem
Cluster 2	12,051	26	42	39	R	Superior and middle frontal gyrus; mid orbital gyrus; superior medial gyrus; SMA [BA 6]
Cluster 3	2381	46	−75	26	R	Inferior parietal cortex [PGp, PGa]; middle temporal and occipital gyrus; angular gyrus
Cluster 4	1384	3	−60	64	R/L	Superior parietal lobule [7A; 7P; 7M]; precuneus
Cluster 5	359	−15	33	48	L	Superior frontal gyrus
Cluster 6	222	69	−6	−22	R	Middle temporal gyrus
Cluster 7	189	3	−56	3	R	Cerebellum [lobule: 10% V]; precuneus
Conjunction: anterior and posterior cerebellar seeds						
Cluster 1	29,114	0	−69	−38	L	Cerebellum [15% VIIa (Crus I, II); 13.4% VI; 2% VIIIA, 1% VIIIB; 1% VIIb; 3% V; 2% IX–X; 1% I–IV]; brainstem
					R	Cerebellum [21% VIIa (Crus I, II); 13% VI; 2% VIIIA, 1% VIIIB; 1% VIIb; 3% V; 2% IX–X; 1% I–IV]; brainstem
Contrast: anterior > posterior cerebellar seed						
Cluster 1	9566	−3	−58	−12	L	Cerebellum [5% V; 5% I–IV; 5% VI]; brainstem; thalamus; caudate; putamen; pallidum; visual cortex [hOC4v, V4; hOC3v, V3v; BA 18]
					R	Cerebellum [7% V; 5% I–IV; 4% VI; 0.5% VIIa (Crus I)–VIIIA]; brainstem; thalamus; caudate; putamen; pallidum; hippocampus [SUB] visual cortex [BA 18; hOC3v, V3v]
Cluster 2	5003	32	−28	52	R	Precentral gyrus, M1 [BA 4p, 4a], PMC [BA 6]; postcentral gyrus, SI [BA 3b, 3a, 1, 2]; inferior parietal cortex [PFt]
Cluster 3	4098	−30	−32	58	L	Precentral gyrus, M1 [BA 4p, 4a], PMC [BA 6]; postcentral gyrus, SI [BA 3b, 3a, 1, 2]; superior parietal lobule [5L]
Cluster 4	1675	−22	48	24	L	Middle frontal gyrus; superior frontal gyrus
Cluster 5	1069	3	−28	56	R/L	Precentral gyrus, M1 [BA 4a], SMA [BA 6]
Cluster 6	720	−28	−39	−3	L	Hippocampus [CA; FD]; parahippocampal gyrus; thalamus
Cluster 7	606	33	−52	−2	R	Hippocampus [CA; FD]; parahippocampal gyrus
Cluster 8	503	−8	−104	0	L	Visual cortex [BA 17, 18]
Cluster 9	234	−12	34	10	L	Anterior cingulate
Cluster 10	185	40	−12	6	R	Insula [Ig2]; parietal operculum, SII [OP1, OP4]
Contrast: anterior < posterior cerebellar seed						
Cluster 1	11,073	26	42	39	R/L	Middle and superior frontal gyrus; superior medial gyrus;
					R	Middle and superior orbital gyrus
Cluster 2	5654	−6	−75	−40	L	Cerebellum [55% VIIa (Crus I, II), 5% VIIb; 1% VI; 0.5% VIIIA]
					R	Cerebellum [14% VIIa (Crus I, II), 1% VIIb; 1% VIIIA]
Cluster 3	2381	46	−75	26	R	Inferior parietal cortex [PGp; PGa]; middle temporal and occipital gyrus; angular gyrus
Cluster 4	2341	−6	−58	−48	L	Cerebellum [17% IX; 2% I–IV; 2% X; 1.5% VIIIB]; brainstem
					R	Cerebellum [14% IX; 2% VIIIB; 1% X]; brainstem
Cluster 5	1384	3	−60	64	R/L	Superior parietal lobule [7A; 7P; 7M; 5L]; precuneus
Cluster 6	222	69	−6	−22	R	Middle temporal gyrus
Cluster 7	132	2	−50	10	R	Cerebellum; precuneus
Cluster 8	72	57	−45	−52	R	Cerebellum [8% VIIa, Crus I]
Cluster 9	62	−16	28	51	L	Superior frontal and medial gyrus

k_E: cluster extent; Lat.: laterality; L: left; R: right; M1: primary motor cortex; PMC: premotor cortex; SMA: supplementary motor area; SI: primary somatosensory cortex, SII: secondary somatosensory cortex.

[a] Cluster maxima.

Table 3
Conjunction between task-based MACM and task-free resting state functional connectivity.

Cluster #	k_E	MNI co-ordinates[a]			Lat.	Macroanatomical and cytoarchitectonic region
		x	y	z		
Conjunction between MACM and resting state for anterior cerebellar seed						
Cluster 1	7453	1	−56	−21	L	Cerebellum [25% VI; 12% V; 3% I–IV; 1% VIIb–VIIIA]; visual cortex [hOC4v, V4]
					R	Cerebellum [27% VI; 15% V; 3% VIIIA, 0.5% VIIIB; 2% I–IV; 1% VIIa, Crus I]; visual cortex [BA 18]
Cluster 2	1423	−46	−30	44	L	Postcentral gyrus, SI [BA 3b, 3a, 1, 2]; precentral gyrus, M1 [BA 4p, 4a], PMC [BA 6]
Cluster 3	571	45	−30	39	R	Inferior parietal cortex [PFt]; precentral gyrus, M1 [BA 4p, 4a], PMC [BA 6]; postcentral gyrus, SI [BA 3b, 3a, 1, 2]
Cluster 4	336	0	−14	50	R/L	Precentral gyrus, SMA [BA 6]
Cluster 5	286	4	−22	−9	R/L	Thalamus
Conjunction between MACM and resting state for posterior cerebellar seed						
Cluster 1	3045	−10	−67	−39	L	Cerebellum [17% VIIIA, 8% VIIIB; 10% VIIa (Crus I, II),9% VIIb; 11% IX; 5% VI];
					R	Cerebellum [3% VIIIA, 1% VIIIB; 2% IX]
Cluster 2	546	14	−62	−33	R	Cerebellum [90% VI]
Cluster 3	294	−38	−56	−34	L	Cerebellum [54% VIIa, Crus I; 46% VI]
Cluster 4	24	39	−57	−27	R	Cerebellum [83% VI]
Conjunction between MACM AND Resting state contrasts: anterior > posterior seed						
Cluster 1	456	−36	−24	53	L	Precentral gyrus, M1 [BA 4p, 4a], PMC [BA 6]; postcentral gyrus, SI [BA 3b, 3a, 1, 2]
Cluster 2	233	8	−48	−18	R	Cerebellum [36% V; 14% VI; 6% I–IV]
					L	Cerebellum [21% V; 17% VI; 3% I–IV]
Cluster 3	63	32	−24	48	R	Precentral gyrus, M1 [BA 4p, 4a], PMC [BA 6]
Cluster 4	52	0	−16	50	L	Precentral gyrus, SMA [BA 6]
Cluster 5	36	4	−22	−8	R	Thalamus
Cluster 6	34	44	−32	40	R	Inferior parietal cortex [PFt]; postcentral gyrus, SI [BA 2, 3b]
Cluster 7	24	16	−52	−28	R	Cerebellum [45% V]
Conjunction between MACM and resting state contrasts: anterior < posterior seed						
Cluster 1	120	−10	−75	−42	L	Cerebellum [42% VIIb, 18% VIIa (Crus II); 18% VIIIA]
Cluster 2	29	−28	−66	−50	L	Cerebellum [54% VIIb; 10% VIIIA]
Cluster 3	22	−8	−58	−48	L	Cerebellum [84% IX]

k_E: cluster extent; Lat.: laterality; L: left; R: right; M1: primary motor cortex; PMC: premotor cortex; SMA: supplementary motor area; SI: primary somatosensory cortex.
[a] Cluster maxima.

shown numerous times, using different techniques to assess structure and metabolic features (Gunther et al., 2004; Lasek et al., 2006; Loy et al., 2005; Toyoshima et al., 2004). Therefore, the finding of basal ganglia connectivity, even though at slightly different location across both approaches, fits very well into the context of previous studies. Clinically, it has moreover been shown that the spasticity and UPDRS-III score were negatively correlated with the putaminal volume (Lasek et al., 2006). On that account the affected basal ganglia and their putatively disturbed connections may reflect the extrapyramidal signs such as dystonia, chorea and parkinsonism in SCA17.

Finally, further corroborating functional implications of the demonstrated connections to sensory-motor areas, the functional characterization of the cerebellar anterior seed using the meta-data of the experiments in BrainMap confirmed the notion that the anterior cerebellar atrophy may underlie motor related symptoms in SCA17. All behavioral domains and paradigm classes that were significantly overrepresented in experiments related to the cerebellar anterior cluster were mainly involved in motor function (action, execution, finger tapping).

Taken together, we found functional connectivity of the cerebellar anterior seed with mainly motor-related cerebellar and cortical areas as well as functional involvement particularly in motor-related tasks. Linking this evidence to the neurodegenerative disorder SCA17, the observed atrophy of the anterior cerebellum and its revealed cerebello-cerebral and cerebello-thalamo-cerebral connections, probably leads inter alia to the main clinical motor deficits such as ataxia, extrapyramidal symptoms and dystonia in SCA17 patients (Hernandez et al., 2003; Lasek et al., 2006; Nakamura et al., 2001; Reetz et al., 2010, 2011; Zuhlke et al., 2001).

Connectivity and function of the cerebellar posterior seed

Consistent functional connectivity for the cerebellar posterior cluster across both analyses was found within the cerebellum, in lobules VI–IX. In contrast to the highly consistent functional connectivity analyses of cerebellar anterior seed, however, no more consistent functional connectivity with cortical regions was found for the cerebellar posterior cluster. The low overlap between MACM and resting-state analyses for the posterior seed may be due to the low pass filter setting used in the resting state analysis. We used standard filter bands (0.01–0.08 Hz) for resting state analyses, however, it can be suggested that transmodal cortical regions oscillate at higher frequencies than sensory regions (Baria et al., 2011). This may lead to losing some signal which in turn may lead to the false negatives in the conjunction. However, it should be further reiterated, that in spite of their common focus on functional connectivity, the two employed approaches focus on very different aspects of this notion (Eickhoff and Grefkes, 2011). Whereas meta-analytic connectivity modeling assessed functional coupling in the presence of externally purported, goal-directed tasks, resting-state functional connectivity analysis investigates coupling in an endogenously controlled state of unconstrained cognition (Schilbach et al., 2012). It may be argued, that convergent findings across both approaches might represent the core of the respective network-interactions. Non-converging findings, in turn, may reflect the fundamental differences in the current "mode" of brain function and hence differences in functional interactions in these states (externally structured or endogenously controlled). Nevertheless, it is noteworthy, that task-based MACM and task free resting state analyses both revealed functional connectivity of the posterior cerebellar seed with fronto-temporo-parietal structures. At this, task-based MACM also showed functional connectivity in the middle cingulate cortex, the precentral and inferior frontal gyrus, the anterior insula and the thalamus. Task free resting state analyses additionally indicated functional connectivity in the parietal association cortex including the precuneus. In line with this less distinct and convergent pattern but also resonating well with the revealed coupling to multi-modal association areas, functional characterization of the cerebellar posterior cluster showed less

specificity, but was predominantly associated with attention-related cognitive tasks (i.e., action observation, instruction of attention).

In contrast to the more motor-related cerebellar anterior lobe, it has been suggested that the cerebellar posterior lobe also contributes to complex cognitive operations, while in particular the posterior aspects of the cerebellar vermis are engaged in affective processing (Exner et al., 2004; Levisohn et al., 2000; Schmahmann, 2004; Schmahmann and Sherman, 1998; Schoch et al., 2006; Tavano et al., 2007). At this, it has to be also acknowledged, that the posterior lobe most likely involves both functions (motor and cognitive/affective) and that an additional motor seed region or rather a dichotomy within the motor system exists (Rathelot and Strick, 2009). That in particular, the posterior cerebellum is also involved in nonmotor functions, modifying the traditional view suggesting predominantly motor functions for the cerebellum (Leiner et al., 1986). Indeed, a growing number of conventional tracing technique studies in non-human primates (Middleton and Strick, 1994; Schmahmann and Pandya, 1997a) and lesions as well as structural and functional neuroimaging studies in humans suggest more recently a role for the cerebellum in cognition and emotion (e.g. O'Reilly et al., 2008; Ravizza et al., 2006; Schmahmann, 2004). As in particular, the cerebellar posterior lobe and its connections is associated with higher-level cognitive function it may – if affected – illustrates the neuronal correlate of the manifestation of cognitive deficits up to dementia, as part of the neuropsychiatric profile in SCA17 patients. The occurrence of cognitive deficits and dementia in this neurodegenerative disorder has in turn been described several times (De Michele et al., 2003; Hernandez et al., 2003; Lasek et al., 2006; Rolfs et al., 2003).

A broad spectrum of deficits in cognitive and emotional demanding neuropsychiatric domains such as dementia, a personality change, reduced global psychiatric functioning and also phobia, dysthymia, adjustment disorder and obsessive–compulsive disorder, has been clinically observed in SCA17 patients, including the sample morphologically investigated here (Lasek et al., 2006; Reetz et al., 2010). At this, we have further shown that the observed personality changes and partly also reduced global psychiatric functioning in SCA17 were highly associated with atrophy in fronto-parietal (including the insula) and limbic (anterior and posterior cingulate cortex) systems (Lasek et al., 2006), areas that are functionally linked to attentional, motivational and emotional processing (Cavanna and Trimble, 2006; Davis et al., 2005; Heinzel et al., 2005). In addition, the insula has been linked to social–emotional, sensorimotor, the olfacto-gustatory, and cognitive networks of the brain (Kurth et al., 2010b). Supporting this, an intrinsic functional connectivity study showed that a large portion of the posterior hemispheres of the cerebellum were connected to with the prefrontal cortex (Krienen and Buckner, 2009). Consequently, neurodegeneration in terms of atrophy and their connections must be held responsible for the observed clinical neuropsychiatric deficits.

The consideration that extensive portions of the posterior cerebellum are also associated with putatively "cognitive" networks is especially interesting in light of the suggestion that phylogenetic expansion of certain lateral and posterior aspects of the cerebellum and cerebellar nuclei has paralleled the expansion of the frontal cortex (MacLeod et al., 2003; Rilling and Insel, 1998; Whiting and Barton, 2003) and also the thalamus (Whiting and Barton, 2003). Interestingly, the default mode network (DMN), which involves the posterior cingulate/precuneus, medial prefrontal/cingulate cortices, temporo-parietal regions, and medial temporal lobes (Greicius et al., 2003; Raichle et al., 2001), was also found in lobule IX, whose functional significance remains still unresolved, (Filippini et al., 2009; Habas et al., 2009) and the right lobule VIIb (Habas et al., 2009). In that view, it is interesting, that the DMN plays a putative role in episodic memory retrieval and self-reflection.

Task-based functional connectivity revealed again further connectivity to the thalamus. Here, peculiar cerebello-thalamo-cerebral connections to mainly prefrontal and temporal cortices were exposed. In the context of non-motor functions, this pathway is the primary feedback loop from the cerebellum to the frontal cortex (Middleton and Strick, 2001; Schmahmann, 1996). Specifically, cerebello-thalamo-cerebral pathways, connecting the cerebellum and the dorsolateral prefrontal cortex (DLPFC), which have been documented well in animal and human models (Dum and Strick, 2003; Middleton and Strick, 2001; Schmahmann and Pandya, 1997b), play an crucial role in the cognitive functioning including working memory (Law et al., 2011), reflecting back well onto the functional characterization of the posterior cerebellar cluster in the present study.

In particular with respect to the finding of the parietal association cortex including the precuneus, revealed by functional connectivity analyses, it is interesting to note that the precuneus is located in the postero-medial portion of the parietal lobe and has a complex set of interconnections, namely multiple reciprocal and afferent/efferent cortical connections to the cingulate, the adjacent parietal and frontal cortex and subcortical projections to the thalamus, striatum, claustrum as well as the brainstem (Cavanna and Trimble, 2006). According to the interwoven network, the precuneus most likely plays an important role in the modulation of self-processing, consciousness, episodic memory retrieval and visuo-spatial imagery (Cavanna and Trimble, 2006), potentially mirroring disturbed clinical neuropsychiatric deficits in SCA17 patients.

Overall, the functional connectivity analyses revealed extensive interactions of the cerebellar posterior seed with mainly cognitive/affective-related brain structures. Thus, it can be implicit that the disruption of these cerebello-(thalamo)-cerebral connections by atrophy of the posterior cerebellum may underlie to the cognitive and emotional/affective deficits commonly observed in SCA17 patients. The present analysis thus indicated that by virtue of the interconnection with different brain regions, the two clusters revealed as atrophic in SCA17 by morphometric analysis may contribute differentially to the clinical spectrum of this disorder. The innovation carried by this paper should be twofold. First, we now provided a link between clinical information in a disorder marked by cerebellar atrophy and the previous findings on cerebellar heterogeneity. Second, any maybe even more important, we here present and illustrate a new approach to supplement specific information on function and connectivity to morphometric findings. Hereby, the purely anatomical findings in VBM studies can now be complemented with information on task-based and task-independent functional connectivity as well as behavioral characterizations, allowing an unprecedented avenue to interpret structural alternations.

Conclusion

In the present study, we used functional connectivity modeling of interactions in task-free and task-driven states as well as database-driven functional attribution to further characterize the loci of morphometric findings in SCA17. Using this multi-modal approach, we demonstrated a robust distinction in the functional connectivity of these two cerebellar regions that could be linked to differences in functional properties. Whereas the cerebellar anterior cluster showed consistent functional connectivity with mainly motor-related areas, the cerebellar posterior seed was coupled with more cognitive/emotional-related fronto-temporo-parietal areas. These results mirror not only the brunt of motor but also the broad spectrum of neuropsychiatric deficits in SCA17, and does not only provide additional valuable information about probably disrupted cerebellar-(thalamo-)cerebral connections in this disorder but moreover also supports the hypothesis of a dichotomy of the human cerebellum.

Funding

KR, ID and SBE were funded by the Excellence Initiative of the German federal and state governments. We acknowledge funding by the Human

Brain Project (R01-MH074457-01A1; PTF, ARL, SBE), and the Helmholtz Initiative on Systems-Biology "The Human Brain Model" (SBE).

Appendix A. Supplementary data

Supplementary data to this article can be found online at http://dx.doi.org/10.1016/j.neuroimage.2012.05.058.

References

Amunts, K., Schleicher, A., Burgel, U., Mohlberg, H., Uylings, H.B., Zilles, K., 1999. Broca's region revisited: cytoarchitecture and intersubject variability. J. Comp. Neurol. 412, 319–341.

Amunts, K., Malikovic, A., Mohlberg, H., Schormann, T., Zilles, K., 2000. Brodmann's areas 17 and 18 brought into stereotaxic space-where and how variable? Neuroimage 11, 66–84.

Amunts, K., Kedo, O., Kindler, M., Pieperhoff, P., Mohlberg, H., Shah, N.J., Habel, U., Schneider, F., Zilles, K., 2005. Cytoarchitectonic mapping of the human amygdala, hippocampal region and entorhinal cortex: intersubject variability and probability maps. Anat. Embryol. (Berl) 210, 343–352.

Ashburner, J., Friston, K.J., 2005. Unified segmentation. Neuroimage 26, 839–851.

Baria, A.T., Baliki, M.N., Parrish, T., Apkarian, A.V., 2011. Anatomical and functional assemblies of brain BOLD oscillations. J. Neurosci. 31, 7910–7919.

Behrens, T.E., Johansen-Berg, H., Woolrich, M.W., Smith, S.M., Wheeler-Kingshott, C.A., Boulby, P.A., Barker, G.J., Sillery, E.L., Sheehan, K., Ciccarelli, O., Thompson, A.J., Brady, J.M., Matthews, P.M., 2003. Non-invasive mapping of connections between human thalamus and cortex using diffusion imaging. Nat. Neurosci. 6, 750–757.

Behzadi, Y., Restom, K., Liau, J., Liu, T.T., 2007. A component based noise correction method (CompCor) for BOLD and perfusion based fMRI. Neuroimage 37, 90–101.

Biswal, B., Yetkin, F.Z., Haughton, V.M., Hyde, J.S., 1995. Functional connectivity in the motor cortex of resting human brain using echo-planar MRI. Magn. Reson. Med. 34, 537–541.

Bostan, A.C., Dum, R.P., Strick, P.L., 2010. The basal ganglia communicate with the cerebellum. Proc. Natl. Acad. Sci. U.S.A. 107, 8452–8456.

Bower, J.M., 1997. Control of sensory data acquisition. Int. Rev. Neurobiol. 41, 489–513.

Bruni, A.C., Takahashi-Fujigasaki, J., Maltecca, F., Foncin, J.F., Servadio, A., Casari, G., D'Adamo, P., Maletta, R., Curcio, S.A., De Michele, G., Filla, A., El Hachimi, K.H., Duyckaerts, C., 2004. Behavioral disorder, dementia, ataxia, and rigidity in a large family with TATA box-binding protein mutation. Arch. Neurol. 61, 1314–1320.

Buckner, R.L., Krienen, F.M., Castellanos, A., Diaz, J.C., Yeo, B.T., 2011. The organization of the human cerebellum estimated by intrinsic functional connectivity. J. Neurophysiol. 106, 2322–2345.

Burk, K., Globas, C., Bosch, S., Klockgether, T., Zuhlke, C., Daum, I., Dichgans, J., 2003. Cognitive deficits in spinocerebellar ataxia type 1, 2, and 3. J. Neurol. 250, 207–211.

Caspers, S., Eickhoff, S.B., Geyer, S., Scheperjans, F., Mohlberg, H., Zilles, K., Amunts, K., 2008. The human inferior parietal lobule in stereotaxic space. Brain Struct. Funct. 212, 481–495.

Caspers, S., Zilles, K., Laird, A.R., Eickhoff, S.B., 2010. ALE meta-analysis of action observation and imitation in the human brain. Neuroimage 50, 1148–1167.

Cavanna, A.E., Trimble, M.R., 2006. The precuneus: a review of its functional anatomy and behavioural correlates. Brain 129, 564–583.

Chai, X.J., Castanon, A.N., Ongur, D., Whitfield-Gabrieli, S., 2012. Anticorrelations in resting state networks without global signal regression. Neuroimage 59, 1420–1428.

Choi, H.J., Zilles, K., Mohlberg, H., Schleicher, A., Fink, G.R., Armstrong, E., Amunts, K., 2006. Cytoarchitectonic identification and probabilistic mapping of two distinct areas within the anterior ventral bank of the human intraparietal sulcus. J. Comp. Neurol. 495, 53–69.

D'Agata, F., Caroppo, P., Baudino, B., Caglio, M., Croce, M., Bergui, M., Tamietto, M., Mortara, P., Orsi, L., 2011a. The recognition of facial emotions in spinocerebellar ataxia patients. Cerebellum 10, 600–610.

D'Agata, F., Caroppo, P., Boghi, A., Coriasco, M., Caglio, M., Baudino, B., Sacco, K., Cauda, F., Geda, E., Bergui, M., Geminiani, G., Bradac, G.B., Orsi, L., Mortara, P., 2011b. Linking coordinative and executive dysfunctions to atrophy in spinocerebellar ataxia 2 patients. Brain Struct. Funct. 216, 275–288.

Davis, K.D., Taylor, K.S., Hutchison, W.D., Dostrovsky, J.O., McAndrews, M.P., Richter, E.O., Lozano, A.M., 2005. Human anterior cingulate cortex neurons encode cognitive and emotional demands. J. Neurosci. 25, 8402–8406.

De Michele, G., Maltecca, F., Carella, M., Volpe, G., Orio, M., De Falco, A., Gombia, S., Servadio, A., Casari, G., Filla, A., Bruni, A., 2003. Dementia, ataxia, extrapyramidal features, and epilepsy: phenotype spectrum in two Italian families with spinocerebellar ataxia type 17. Neurol. Sci. 24, 166–167.

Diedrichsen, J., 2006. A spatially unbiased atlas template of the human cerebellum. Neuroimage 33, 127–138.

Diedrichsen, J., Balsters, J.H., Flavell, J., Cussans, E., Ramnani, N., 2009. A probabilistic MR atlas of the human cerebellum. Neuroimage 46, 39–46.

Dum, R.P., Strick, P.L., 2003. An unfolded map of the cerebellar dentate nucleus and its projections to the cerebral cortex. J. Neurophysiol. 89, 634–639.

Eickhoff, S.B., Grefkes, C., 2011. Approaches for the integrated analysis of structure, function and connectivity of the human brain. Clin. EEG Neurosci. 42, 107–121.

Eickhoff, S.B., Stephan, K.E., Mohlberg, H., Grefkes, C., Fink, G.R., Amunts, K., Zilles, K., 2005. A new SPM toolbox for combining probabilistic cytoarchitectonic maps and functional imaging data. Neuroimage 25, 1325–1335.

Eickhoff, S.B., Schleicher, A., Zilles, K., Amunts, K., 2006. The human parietal operculum. I. Cytoarchitectonic mapping of subdivisions. Cereb. Cortex 16, 254–267.

Eickhoff, S.B., Paus, T., Caspers, S., Grosbras, M.H., Evans, A.C., Zilles, K., Amunts, K., 2007. Assignment of functional activations to probabilistic cytoarchitectonic areas revisited. Neuroimage 36, 511–521.

Eickhoff, S.B., Heim, S., Zilles, K., Amunts, K., 2009a. A systems perspective on the effective connectivity of overt speech production. Philos. Transact. A Math. Phys. Eng. Sci. 367, 2399–2421.

Eickhoff, S.B., Laird, A.R., Grefkes, C., Wang, L.E., Zilles, K., Fox, P.T., 2009b. Coordinate-based activation likelihood estimation meta-analysis of neuroimaging data: a random-effects approach based on empirical estimates of spatial uncertainty. Hum. Brain Mapp. 30, 2907–2926.

Eickhoff, S.B., Jbabdi, S., Caspers, S., Laird, A.R., Fox, P.T., Zilles, K., Behrens, T.E., 2010. Anatomical and functional connectivity of cytoarchitectonic areas within the human parietal operculum. J. Neurosci. 30, 6409–6421.

Eickhoff, S.B., Bzdok, D., Laird, A.R., Kurth, F., Fox, P.T., 2011. Activation likelihood estimation meta-analysis revisited. Neuroimage 59, 2349–2361.

Eickhoff, S.B., Bzdok, D., Laird, A.R., Kurth, F., Fox, P.T., 2012. Activation likelihood estimation meta-analysis revisited. Neuroimage 59, 2349–2361.

Exner, C., Weniger, G., Irle, E., 2004. Cerebellar lesions in the PICA but not SCA territory impair cognition. Neurology 63, 2132–2135.

Filippini, N., MacIntosh, B.J., Hough, M.G., Goodwin, G.M., Frisoni, G.B., Smith, S.M., Matthews, P.M., Beckmann, C.F., Mackay, C.E., 2009. Distinct patterns of brain activity in young carriers of the APOE-epsilon4 allele. Proc. Natl. Acad. Sci. U.S.A. 106, 7209–7214.

Fox, M.D., Raichle, M.E., 2007. Spontaneous fluctuations in brain activity observed with functional magnetic resonance imaging. Nat. Rev. Neurosci. 8, 700–711.

Geyer, S., 2004. The microstructural border between the motor and the cognitive domain in the human cerebral cortex. Adv. Anat. Embryol. Cell Biol. 174 (I-VIII), 1–89.

Geyer, S., Ledberg, A., Schleicher, A., Kinomura, S., Schormann, T., Burgel, U., Klingberg, T., Larsson, J., Zilles, K., Roland, P.E., 1996. Two different areas within the primary motor cortex of man. Nature 382, 805–807.

Geyer, S., Schleicher, A., Zilles, K., 1999. Areas 3a, 3b, and 1 of human primary somatosensory cortex. Neuroimage 10, 63–83.

Geyer, S., Schormann, T., Mohlberg, H., Zilles, K., 2000. Areas 3a, 3b, and 1 of human primary somatosensory cortex. Part 2. Spatial normalization to standard anatomical space. Neuroimage 11, 684–696.

Graybiel, A.M., 2005. The basal ganglia: learning new tricks and loving it. Curr. Opin. Neurobiol. 15, 638–644.

Grefkes, C., Eickhoff, S.B., Nowak, D.A., Dafotakis, M., Fink, G.R., 2008. Dynamic intra- and interhemispheric interactions during unilateral and bilateral hand movements assessed with fMRI and DCM. Neuroimage 41, 1382–1394.

Greicius, M.D., Krasnow, B., Reiss, A.L., Menon, V., 2003. Functional connectivity in the resting brain: a network analysis of the default mode hypothesis. Proc. Natl. Acad. Sci. U.S.A. 100, 253–258.

Grodd, W., Hulsmann, E., Lotze, M., Wildgruber, D., Erb, M., 2001. Sensorimotor mapping of the human cerebellum: fMRI evidence of somatotopic organization. Hum. Brain Mapp. 13, 55–73.

Gunther, P., Storch, A., Schwarz, J., Sabri, O., Steinbach, P., Wagner, A., Hesse, S., 2004. Basal ganglia involvement of a patient with SCA 17 — a new form of autosomal dominant spinocerebellar ataxia. J. Neurol. 251, 896–897.

Habas, C., Kamdar, N., Nguyen, D., Prater, K., Beckmann, C.F., Menon, V., Greicius, M.D., 2009. Distinct cerebellar contributions to intrinsic connectivity networks. J. Neurosci. 29, 8586–8594.

Hagenah, J.M., Zuhlke, C., Hellenbroich, Y., Heide, W., Klein, C., 2004. Focal dystonia as a presenting sign of spinocerebellar ataxia 17. Mov. Disord. 19, 217–220.

Heinzel, A., Bermpohl, F., Niese, R., Pfennig, A., Pascual-Leone, A., Schlaug, G., Northoff, G., 2005. How do we modulate our emotions? Parametric fMRI reveals cortical midline structures as regions specifically involved in the processing of emotional valences. Brain Res. Cogn. Brain Res. 25, 348–358.

Hernandez, D., Hanson, M., Singleton, A., Gwinn-Hardy, K., Freeman, J., Ravina, B., Doheny, D., Gallardo, M., Weiser, R., Hardy, J., 2003. Mutation at the SCA17 locus is not a common cause of parkinsonism. Parkinsonism Relat. Disord. 9, 317–320.

Hoshi, E., Tremblay, L., Feger, J., Carras, P.L., Strick, P.L., 2005. The cerebellum communicates with the basal ganglia. Nat. Neurosci. 8, 1491–1493.

Jakobs, O., Langner, R., Caspers, S., Roski, C., Cieslik, E.C., Zilles, K., Laird, A.R., Fox, P.T., Eickhoff, S.B., 2012. Across-study and within-subject functional connectivity of a right temporo-parietal junction subregion involved in stimulus-context integration. Neuroimage 60, 2389–2398.

Kelly, R.M., Strick, P.L., 2003. Cerebellar loops with motor cortex and prefrontal cortex of a nonhuman primate. J. Neurosci. 23, 8432–8444.

Koide, R., Kobayashi, S., Shimohata, T., Ikeuchi, T., Maruyama, M., Saito, M., Yamada, M., Takahashi, H., Tsuji, S., 1999. A neurological disease caused by an expanded CAG trinucleotide repeat in the TATA-binding protein gene: a new polyglutamine disease? Hum. Mol. Genet. 8, 2047–2053.

Krienen, F.M., Buckner, R.L., 2009. Segregated fronto-cerebellar circuits revealed by intrinsic functional connectivity. Cereb. Cortex 19, 2485–2497.

Kurth, F., Eickhoff, S.B., Schleicher, A., Hoemke, L., Zilles, K., Amunts, K., 2010a. Cytoarchitecture and probabilistic maps of the human posterior insular cortex. Cereb. Cortex 20, 1448–1461.

Kurth, F., Zilles, K., Fox, P.T., Laird, A.R., Eickhoff, S.B., 2010b. A link between the systems: functional differentiation and integration within the human insula revealed by meta-analysis. Brain Struct. Funct. 214, 519–534.

Laird, A.R., Eickhoff, S.B., Kurth, F., Fox, P.M., Uecker, A.M., Turner, J.A., Robinson, J.L., Lancaster, J.L., Fox, P.T., 2009a. ALE meta-analysis workflows via the BrainMap

database: progress towards a probabilistic functional brain atlas. Front. Neuroinformatics 3, 23.
Laird, A.R., Eickhoff, S.B., Li, K., Robin, D.A., Glahn, D.C., Fox, P.T., 2009b. Investigating the functional heterogeneity of the default mode network using coordinate-based meta-analytic modeling. J. Neurosci. 29, 14496–14505.
Laird, A.R., Eickhoff, S.B., Fox, P.M., Uecker, A.M., Ray, K.L., Saenz Jr., J.J., McKay, D.R., Bzdok, D., Laird, R.W., Robinson, J.L., Turner, J.A., Turkeltaub, P.E., Lancaster, J.L., Fox, P.T., 2011. The BrainMap strategy for standardization, sharing, and meta-analysis of neuroimaging data. BMC Res. Notes 4, 349.
Lasek, K., Lencer, R., Gaser, C., Hagenah, J., Walter, U., Wolters, A., Kock, N., Steinlechner, S., Nagel, M., Zuhlke, C., Nitschke, M.F., Brockmann, K., Klein, C., Rolfs, A., Binkofski, F., 2006. Morphological basis for the spectrum of clinical deficits in spinocerebellar ataxia 17 (SCA17). Brain 129, 2341–2352.
Law, N., Bouffet, E., Laughlin, S., Laperriere, N., Briere, M.E., Strother, D., McConnell, D., Hukin, J., Fryer, C., Rockel, C., Dickson, J., Mabbott, D., 2011. Cerebello-thalamo-cerebral connections in pediatric brain tumor patients: impact on working memory. Neuroimage 56, 2238–2248.
Leiner, H.C., Leiner, A.L., Dow, R.S., 1986. Does the cerebellum contribute to mental skills? Behav. Neurosci. 100, 443–454.
Levisohn, L., Cronin-Golomb, A., Schmahmann, J.D., 2000. Neuropsychological consequences of cerebellar tumour resection in children: cerebellar cognitive affective syndrome in a paediatric population. Brain 123 (Pt 5), 1041–1050.
Loy, C.T., Sweeney, M.G., Davis, M.B., Wills, A.J., Sawle, G.V., Lees, A.J., Tabrizi, S.J., 2005. Spinocerebellar ataxia type 17: extension of phenotype with putaminal rim hyperintensity on magnetic resonance imaging. Mov. Disord. 20, 1521–1523.
MacLeod, C.E., Zilles, K., Schleicher, A., Rilling, J.K., Gibson, K.R., 2003. Expansion of the neocerebellum in Hominoidea. J. Hum. Evol. 44, 401–429.
Maldjian, J.A., Laurienti, P.J., Kraft, R.A., Burdette, J.H., 2003. An automated method for neuroanatomic and cytoarchitectonic atlas-based interrogation of fMRI data sets. Neuroimage 19, 1233–1239.
Maltecca, F., Filla, A., Castaldo, I., Coppola, G., Fragassi, N.A., Carella, M., Bruni, A., Cocozza, S., Casari, G., Servadio, A., De Michele, G., 2003. Intergenerational instability and marked anticipation in SCA-17. Neurology 61, 1441–1443.
Middleton, F.A., Strick, P.L., 1994. Anatomical evidence for cerebellar and basal ganglia involvement in higher cognitive function. Science 266, 458–461.
Middleton, F.A., Strick, P.L., 2001. Cerebellar projections to the prefrontal cortex of the primate. J. Neurosci. 21, 700–712.
Nakamura, K., Jeong, S.Y., Uchihara, T., Anno, M., Nagashima, K., Nagashima, T., Ikeda, S., Tsuji, S., Kanazawa, I., 2001. SCA17, a novel autosomal dominant cerebellar ataxia caused by an expanded polyglutamine in TATA-binding protein. Hum. Mol. Genet. 10, 1441–1448.
Nichols, T., Brett, M., Andersson, J., Wager, T., Poline, J.B., 2005. Valid conjunction inference with the minimum statistic. Neuroimage 25, 653–660.
Nickl-Jockschat, T., Schneider, F., Pagel, A.D., Laird, A.R., Fox, P.T., Eickhoff, S.B., 2010. Progressive pathology is functionally linked to the domains of language and emotion: meta-analysis of brain structure changes in schizophrenia patients. Eur. Arch. Psychiatry Clin. Neurosci. 261 (Suppl. 2), S166–S171.
Nickl-Jockschat, T., Kleiman, A., Schulz, J.B., Schneider, F., Laird, A.R., Fox, P.T., Eickhoff, S.B., Reetz, K., 2011. Neuroanatomic changes and their association with cognitive decline in mild cognitive impairment: a meta-analysis. Brain Struct. Funct. 217, 115–125.
O'Reilly, J.X., Mesulam, M.M., Nobre, A.C., 2008. The cerebellum predicts the timing of perceptual events. J. Neurosci. 28, 2252–2260.
O'Reilly, J.X., Beckmann, C.F., Tomassini, V., Ramnani, N., Johansen-Berg, H., 2010. Distinct and overlapping functional zones in the cerebellum defined by resting state functional connectivity. Cereb. Cortex 20, 953–965.
Raichle, M.E., MacLeod, A.M., Snyder, A.Z., Powers, W.J., Gusnard, D.A., Shulman, G.L., 2001. A default mode of brain function. Proc. Natl. Acad. Sci. U.S.A. 98, 676–682.
Rathelot, J.A., Strick, P.L., 2009. Subdivisions of primary motor cortex based on cortico-motoneuronal cells. Proc. Natl. Acad. Sci. U.S.A. 106, 918–923.
Ravizza, S.M., McCormick, C.A., Schlerf, J.E., Justus, T., Ivry, R.B., Fiez, J.A., 2006. Cerebellar damage produces selective deficits in verbal working memory. Brain 129, 306–320.
Reetz, K., Lencer, R., Hagenah, J.M., Gaser, C., Tadic, V., Walter, U., Wolters, A., Steinlechner, S., Zuhlke, C., Brockmann, K., Klein, C., Rolfs, A., Binkofski, F., 2010. Structural changes associated with progression of motor deficits in spinocerebellar ataxia 17. Cerebellum 9, 210–217.
Reetz, K., Kleiman, A., Klein, C., Lencer, R., Zuehlke, C., Brockmann, K., Rolfs, A., Binkofski, F., 2011. CAG repeats determine brain atrophy in spinocerebellar ataxia 17: a VBM study. PLoS One 6, e15125.
Rilling, J.K., Insel, T.R., 1998. Evolution of the cerebellum in primates: differences in relative volume among monkeys, apes and humans. Brain Behav. Evol. 52, 308–314.
Robinson, J.L., Laird, A.R., Glahn, D.C., Lovallo, W.R., Fox, P.T., 2010. Metaanalytic connectivity modeling: delineating the functional connectivity of the human amygdala. Hum. Brain Mapp. 31, 173–184.
Rolfs, A., Koeppen, A.H., Bauer, I., Bauer, P., Buhlmann, S., Topka, H., Schols, L., Riess, O., 2003. Clinical features and neuropathology of autosomal dominant spinocerebellar ataxia (SCA17). Ann. Neurol. 54, 367–375.
Rottschy, C., Eickhoff, S.B., Schleicher, A., Mohlberg, H., Kujovic, M., Zilles, K., Amunts, K., 2007. Ventral visual cortex in humans: cytoarchitectonic mapping of two extrastriate areas. Hum. Brain Mapp. 28, 1045–1059.
Rottschy, C., Langner, R., Dogan, I., Reetz, K., Laird, A.R., Schulz, J.B., Fox, P.T., Eickhoff, S.B., 2012. Modelling neural correlates of working memory: a coordinate-based meta-analysis. Neuroimage 60, 830–846.
Scheperjans, F., Hermann, K., Eickhoff, S.B., Amunts, K., Schleicher, A., Zilles, K., 2008. Observer-independent cytoarchitectonic mapping of the human superior parietal cortex. Cereb. Cortex 18, 846–867.
Schilbach, L., Bzdok, D., Timmermans, B., Fox, P.T., Laird, A.R., Vogeley, K., Eickhoff, S.B., 2012. Introspective minds: using ALE Meta-analyses to study commonalities in the neural correlates of emotional processing, social & unconstrained cognition. PLoS One 7, e30920.
Schmahmann, J.D., 1996. From movement to thought: anatomic substrates of the cerebellar contribution to cognitive processing. Hum. Brain Mapp. 4, 174–198.
Schmahmann, J.D., 2004. Disorders of the cerebellum: ataxia, dysmetria of thought, and the cerebellar cognitive affective syndrome. J. Neuropsychiatry Clin. Neurosci. 16, 367–378.
Schmahmann, J.D., Pandya, D.N., 1997a. Anatomic organization of the basilar pontine projections from prefrontal cortices in rhesus monkey. J. Neurosci. 17, 438–458.
Schmahmann, J.D., Pandya, D.N., 1997b. The cerebrocerebellar system. Int. Rev. Neurobiol. 41, 31–60.
Schmahmann, J.D., Sherman, J.C., 1997. Cerebellar cognitive affective syndrome. Int. Rev. Neurobiol. 41, 433–440.
Schmahmann, J.D., Sherman, J.C., 1998. The cerebellar cognitive affective syndrome. Brain 121 (Pt 4), 561–579.
Schoch, B., Dimitrova, A., Gizewski, E.R., Timmann, D., 2006. Functional localization in the human cerebellum based on voxelwise statistical analysis: a study of 90 patients. Neuroimage 30, 36–51.
Snider, R., Eldred, E., 1951. Electro-anatomical studies on cerebro-cerebellar connections in the cat. J. Comp. Neurol. 95, 1–16.
Stoodley, C.J., Schmahmann, J.D., 2009. Functional topography in the human cerebellum: a meta-analysis of neuroimaging studies. Neuroimage 44, 489–501.
Stoodley, C.J., Valera, E.M., Schmahmann, J.D., 2012. Functional topography of the cerebellum for motor and cognitive tasks: an fMRI study. Neuroimage 59, 1560–1570.
Tavano, A., Grasso, R., Gagliardi, C., Triulzi, F., Bresolin, N., Fabbro, F., Borgatti, R., 2007. Disorders of cognitive and affective development in cerebellar malformations. Brain 130, 2646–2660.
Tedesco, A.M., Chiricozzi, F.R., Clausi, S., Lupo, M., Molinari, M., Leggio, M.G., 2011. The cerebellar cognitive profile. Brain 134, 3669–3683.
Timmann, D., Daum, I., 2007. Cerebellar contributions to cognitive functions: a progress report after two decades of research. Cerebellum 6, 159–162.
Toyoshima, Y., Yamada, M., Onodera, O., Shimohata, M., Inenaga, C., Fujita, N., Morita, M., Tsuji, S., Takahashi, H., 2004. SCA17 homozygote showing Huntington's disease-like phenotype. Ann. Neurol. 55, 281–286.
Turkeltaub, P.E., Eden, G.F., Jones, K.M., Zeffiro, T.A., 2002. Meta-analysis of the functional neuroanatomy of single-word reading: method and validation. Neuroimage 16, 765–780.
Turkeltaub, P.E., Eickhoff, S.B., Laird, A.R., Fox, M., Wiener, M., Fox, P., 2012. Minimizing within-experiment and within-group effects in Activation Likelihood Estimation meta-analyses. Hum. Brain Mapp. 33, 1–13.
Whiting, B.A., Barton, R.A., 2003. The evolution of the cortico-cerebellar complex in primates: anatomical connections predict patterns of correlated evolution. J. Hum. Evol. 44, 3–10.
Zu Eulenburg, P., Caspers, S., Roski, C., Eickhoff, S.B., 2011. Meta-analytical definition and functional connectivity of the human vestibular cortex. Neuroimage 60, 162–169.
Zuhlke, C., Hellenbroich, Y., Dalski, A., Kononowa, N., Hagenah, J., Vieregge, P., Riess, O., Klein, C., Schwinger, E., 2001. Different types of repeat expansion in the TATA-binding protein gene are associated with a new form of inherited ataxia. Eur. J. Hum. Genet. 9, 160–164.